Calibration-Free Calorimeter for Sensitive Loss Measurements: Case of High-Frequency Inductors

Armin Jafari*, Michaël Heijnemans, Reza Soleimanzadeh, Remco van Erp, Mohammad Samizadeh Nikoo, Enea Figini, Furkan Karakaya, Nirmana Perera and *Elison Matioli
Power and Wide-band-gap Electronics Research Laboratory (POWERlab)
École polytechnique fédérale de Lausanne (EPFL)
Lausanne, Switzerland
*armin.jafari@epfl.ch, *elison.matioli@epfl.ch

***Abstract*— Wide-band-gap technologies enable ultra-high efficiencies in high-frequency power conversion. However, inadequate accuracies in electrical measurements could lead to spurious efficiency measurements, even above 100%. Furthermore, bandwidth limitations, particularly for current probing, delay mismatches between current and voltage probes, loading effects and electromagnetic interferences make electrical techniques inappropriate for measuring extremely-low losses in switches with high *dv/dt* and *di/dt* values and magnetic components with high-frequency excitations. Calorimetric methods overcome this issue by a direct loss measurement through the generated heat. Nevertheless, limited ranges and accuracies of existing systems hinder their application in sensitive measurements. Moreover, time-consuming calibrations with extensive data processing impede rapid design assessments. In this work, we further investigate a previously proposed closed-type double-chamber calorimeter and present its high accuracy for the evaluation of low levels of losses in high-frequency power inductors. The system provides adjustable cooling and can measure losses as low as 500 mW, enabling evaluation of high-performance power converters and their components with no dependencies on the geometries of the evaluated devices/systems.**

Keywords*— *Loss measurement, calibration-free, dual-chamber calorimeter, switching losses, magnetic losses, high-frequency passive component losses, wide-band-gap technology, real-time calibration, adjustable cooling capability.

I. Introduction

The emergence of high-performance wide-band-gap (WBG) technologies and high-quality passive components (e.g. high-frequency transformers and inductors) have enabled ultra-high efficiencies in high-frequency power conversion [1]–[8]. However, measuring high efficiencies electrically is prone to large errors due to insufficient measurement accuracies [9], [10]. Furthermore, electrical probes (especially current probes) suffer from limited bandwidths, neglecting the effect of high-order harmonics [4], [11]. Probe burden, propagation delays between voltage and current probes and electromagnetic interference (EMI) are other limiting factors for precise loss measurements in various converter building blocks such as switches with fast transitions and high-frequency magnetic components [9], [10], [12].

Calorimetric methods have been used to directly determine losses from generated heat in power converters [10], [13], pulsed-power generators [14], motors and drives [15], [16], semiconductor devices and passive components [9], [17].

In a calorimetric system, heat-transfer rate (P) to the coolant is determined by

$$P = \rho \left(\frac{dV}{dt}\right) c_{\mathrm{p}}\, \Delta T \qquad (1)$$

in which ρ is volumetric density of the coolant, V is its volume, c_{p} is the isobaric specific heat capacity, and ΔT is the temperature rise. Single-chamber open-type calorimeters use air-flow meters with temperature sensors at the inlet and outlet of a chamber with air blown on the device-under-test (DUT). This method is simple to implement for measuring large losses [18]. Air parameters such as ρ and c_{p} are susceptible to large variations and for reliable measurements, time-consuming calibrations or balance tests must be performed. A balance test is performed with heaters to emulate the operation conditions of the main DUT to compensate for the variations in air properties. Furthermore, heat leakage through the chamber has to be minimized for high precision [15]. A double-chamber open-type calorimeter can mitigate the need for calibrations and balance tests [19]. This method is practical for large losses, but equalizing the heat leakage between the two chambers remains a challenge as there is no guarantee that the airflow remains the same in both chambers, depending on the DUT geometry [12]. By using a heat-exchanger and transferring the heat to a liquid (e.g. water), one can directly extract the power loss by a single chamber closed-type calorimeter using (1) [10], [18], [20]. Although using water with its large heat capacity increases the settling time in closed-type systems, the accuracy is significantly higher. A single-chamber calorimeter must obtain minimized heat leakage through the walls, so the double-jacketing technique is used in [10], [13], [18]. Christen *et al.* reported a good precision of ±0.4 W for a 10-W loss measurement [10]. The calorimeter is suitable for evaluating losses up to 100 W; nonetheless, evaluating lower losses requires a much higher sensitivity. Our proposed double-chamber closed-type calorimeter [21], shown in Fig. 1, overcomes the limitations of the aforementioned methods by:

1) Reducing flow rate drastically for achieving higher sensitivity. The same coolant flows in both chambers, hence, there is no need to measure the extremely low flow rates, which is highly challenging [18]. As a result, the sensitivity is high enough to measure losses as low as 500 mW with significantly lower costs.

This work was supported in part by the Swiss Office of Energy under Grant SI/501887-01 (MEPCO) and in part by the European Research Council (ERC Starting Grant) under the European Union's H2020 Program/ERC Grant Agreement No. 679425.

TABLE I
METHODS USED IN CALORIMETRIC SYSTEMS

Reference	System	Type/ Coolant	Minimum Power	Accuracy	Accuracy Limitation
[18]	Single-chamber	Closed/ Water	74.5 W	±0.5 W	Flowmeter, water temp. sensors
[19]	Double-chamber	Open/ Air	200 W	±15 W	Uneven air flow, air variations
[10]	Single-chamber	Closed/ Water	10 W	Max {±0.4 W, 1%}	Flowmeter, water temp. sensors
This work	Double-chamber	Closed/ Water	500 mW	At 500 mW: +50%/ -30% At 15 W: ± 3%	Water temperature sensors

2) Replacing time-consuming calibrations, balance tests and data processing by a real-time calibration, for faster loss evaluations.
3) Avoiding the need for perfect thermal insulation, since low levels of heat leakage – if equal for both chambers (which holds in the case of designing identical chambers) – do not introduce measurement inaccuracies.

II. METHODOLOGY

The proposed calorimeter [21] enables geometry-independent loss measurements by transferring the heat to the water through heat-exchangers (convection) and cold plates (conduction). Two identical heat-insulated chambers are placed inside an outer chamber that isolates the calorimeter from the ambient (See Fig. 1). The water at ambient temperature flows through the DUT chamber and after absorbing the heat generated by the DUT, gets cooled down to the ambient temperature using an external heat-exchanger. The liquid then flows through the calibration (CAL) chamber and heats up with its dissipated power (P_{CAL}). After the calibration chamber, another external heat-exchanger cools down the liquid to the ambient temperature. The entire heat-transfer cycle is repeated until the temperatures reach steady state. Such a closed loop for the coolant ensures a constant flow in both chambers and eliminates the need for precise flow measurements. Temperature gradients T_4-T_3 and T_2-T_1 are measured and compared constantly, and a PI regulator adjusts P_{CAL}, such that both chambers have equal steady-state temperature gradients. Thus, the DUT losses, P_{DUT}, can be derived at steady state as

$$T_2 - T_1 = T_4 - T_3 \Leftrightarrow P_{DUT} = P_{CAL} \quad (2).$$

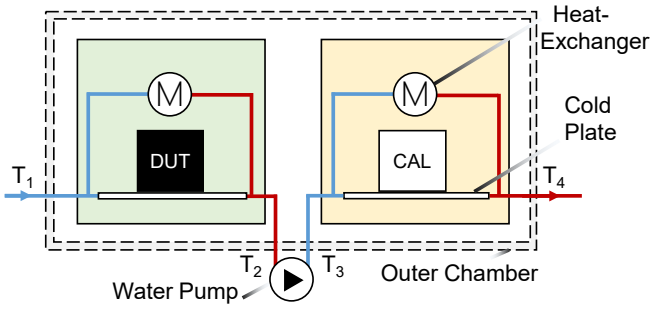

Fig. 1 The proposed calorimeter concept. Water flows in identical chambers containing DUT and CAL. Heat transfers through heat-exchangers (convection) and cold-plates (conduction) and water temperature-rise is measured across both chambers. The blue lines indicate cold water and red lines represent hot water, after absorbing the energy dissipated in DUT and CAL. The arrow shows the direction of flow.

To avoid DUT thermal runaway before steady-state is reached, when (2) can be used for loss evaluation, the cooling capability and sensitivity of the system can be adjusted by changing 1) water-flow rate and 2) fan power of the inner heat-exchangers (P_{FAN}).

This method requires no prior calibration or extra data analysis, resulting in faster evaluation times. TABLE I compares this method with previous techniques in the literature, where our proposed system extends the measurement range to power levels as low as 500 mW.

III. SYSTEM DESIGN

Fig. 2a shows the outer chamber with dimensions 120×66×70 cm^3, made of polystyrene insulator. The water circuit (inset of Fig. 2a) includes a water reservoir connected to a μ-diaphragm pump with a pulsation-damper, to stabilize the low flow of the liquid. Low flow rates enable higher water-temperature rise and thus a higher sensitivity. Inner chambers are consisted of polystyrene boxes with dimensions of 48×42×36 cm^3 and are covered with shielding foils to suppress the effect of EMI from the DUT on the measurements by having the sensors outside the chambers (Fig. 2b). They enclose an aluminum container to hold the inner heat exchangers and the cold plates (see Fig. 2c, d). The DUT is mounted on the cold plate, and its hot-spot temperature (T_{HS}) is monitored through the aperture in the container, using thermal imagers to avoid a thermal runaway. To verify the real-time calibration and its dependence on the DUT geometry, two very different fixtures, *A* and *B*, were employed as shown in Fig. 2e.

The fixture *A* is an array of thick-film resistors mounted on a printed circuit board (PCB). The fixture *B* is a power resistor connected to the cold plate using only one nylon stand-off (with poor thermal conductivity to the cold plate).

Fig. 3a presents general view of the calorimeter and its mechanical components including the inner and outer heat exchangers and the water pump, with the major input (feedback) and output (control) signals indicated. As Fig. 3b shows, a peripheral management board was designed as the interface between the calorimeter and myRio 1900 control unit. Analog and digital grounds were separated in this hardware interface, in order to reduce any EMI issues. The data acquisition system (LabVIEW environment) constantly provided measurements for the real-time regulator as well as the human interface. Moreover, by transferring the data to a computer, all system parameters were recorded for further offline analyses. TABLE II lists a detailed description of all the major calorimeter subcomponents.

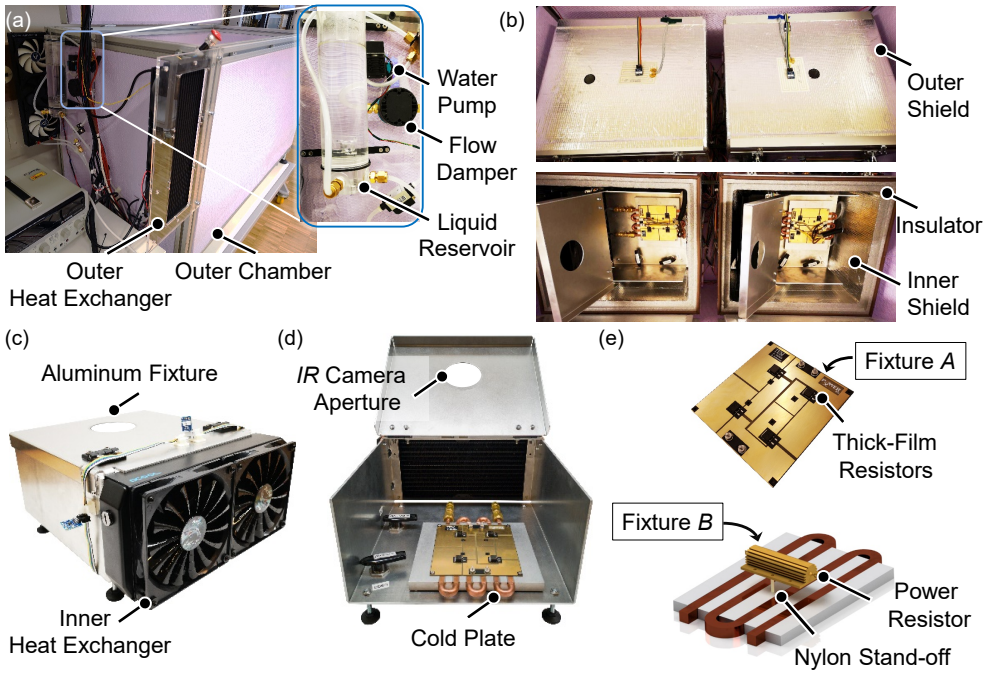

Fig. 2 Calorimeter design. (a) The outer chamber and heat exchangers, together with the water circuit. (b) The inner chambers with the aluminum fixtures inside and shielding foils all over the inner and outer walls to suppress the effect of radiated EMI on the measurements. (c) The container holding inner heat exchangers and cold plates. (d) The back view of the container with resistors mounted on the cold plate. (e) An array of thick-film resistors (Fixture *A*) and a power resistor mounted on the cold plate using only a nylon stand-off (Fixture *B*) are used to examine the dependence of the calorimeter on the DUT geometry, which are evaluated by dc calibrations presented in section IV.

TABLE II
OVERVIEW OF THE CALORIMETER COMPONENTS

Component	Type	Specifications
Water Temp. Sensor	Pt.100 Class AA	Acc. ±0.1 °C
μ-Diaphragm Pump	NFB5KTDCB-4	Max. Pressure = 1 Bar
Pulsation Damper	FPD06KTZ	Max. Pressure = 2 Bar
Cold Plate	416101U00000G	Aluminum/ Copper Tubes
Heat Exchanger In	Alphacool XT45	2 Fans
Heat Exchanger Out	Airplex PRO 240	3 Fans
DC Measurements for Calibrations	Fluke 45	Volt. Acc. 0.025% + 6 Current Acc. 0.2% + 7
DC Measurements for Fan Powers	Fluke 87V	Volt. Acc. 0.05% + 1 Current Acc. 0.2% + 2
Data Acquisition	myRIO-1900	LabVIEW environment

IV. DC CALIBRATION

DC calibrations were performed to verify that both chambers are identical and to ensure that the measurement method has no dependency on the geometry of the DUT [21]. As illustrated in Fig. 4a, using a low flow (minimum pump pressure) enabled adequate sensitivity to losses as low as 100 mW with a mismatch of less than 10% up to 10 W, which is attributed to the temperature measurement errors (see Fig. 4b). A minimum P_{FAN} of 0.3 W was used for homogenous air circulation. We repeated the dc calibrations for a high flow rate, and an error less than 10% was maintained for losses down to 1 W, where the water temperature gradient (ΔT_{Water}) reached the accurate detection threshold of the sensors. As Fig. 4b shows, high flow rates result in lower T_{HS} for the DUT, which can be tuned to avoid its thermal runaway. P_{FAN}

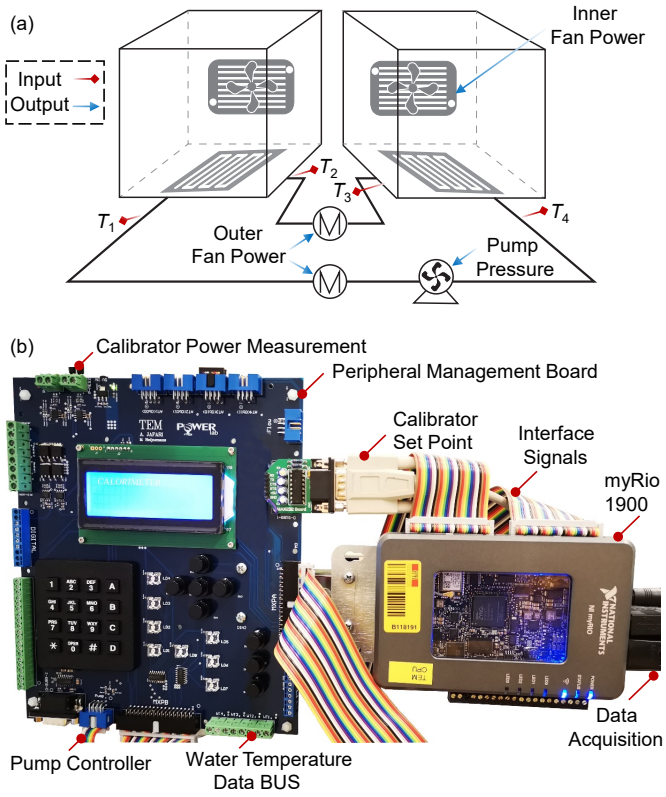

Fig. 3 Control and feedback signals to/from the actuators/sensors. (a) Major input and output signals for the real-time control process and (b) hardware for the controller, including a peripheral management board (left) and myRio 1900 (right). Data acquisition records the measurements on computer for further offline analyses.

is a secondary tunable parameter, for altering convective heat transfer through the inner heat-exchangers. Fig. 4c presents the cases where 5 W and 10 W are consumed by the fans.

As Fig. 4d shows, for P_{FAN} values of up to 10 W, an error much lower than 10% was obtained. To investigate the dependence of the calorimeter on geometry of the heat source, fixtures *A* and *B* were compared. Even with such extreme changes in the geometry of the heat source and its coupling to the system, ΔT_{Water} remained similar (see Fig. 4e), and a maximum error of 10% was obtained (see Fig. 4f), indicating the independent performance of the calorimeter with respect to the DUT geometry.

Fig. 5 presents time-domain temperature gradients of the DUT and CAL chambers in dc calibration (P_{FAN} = 900 mW). The power loss varied from 1 W to 8 W, and slow, medium and fast flows were applied. The calorimeter offer flexibility for measuring DUTs with different cooling requirements.

V. Power Tracking and Accuracy

Fig. 6a presents the transient ΔT_{Water} for both chambers, together with the power tracking in CAL, when DUT is dissipating 7.8 W. A proportional-integral (PI) regulator provided the reference power (P^*_{CAL}) to a dc source to satisfy (2), as shown in Figs. 6b, c.

The system constantly monitored T_{HS} in the chambers and limited the power to the CAL and DUT to avoid thermal runaway. The proportional (k_P) and integral (k_I) coefficients were set to tune the power tracking transient. The power is measured by multiplying the voltage and current of the calibrator using Fluke 45 multimeter as

$$P_{CAL} = (V_{CAL} \pm \varepsilon_V)(I_{CAL} \pm \varepsilon_I) \quad (3)$$

in which ε_V = 0.025% and ε_I = 0.2% are the dc voltage and dc current measurement errors, respectively. At steady state, the temperature rise in the water is linearly proportional to the dissipated power (see the left-side curves in Fig. 3, and note that the power is in logarithmic scale). Based on (2) and (3), one can extract the tracked power (P_{TRACK}) as

$$P_{TRACK} = P_{LOSS}(1 \pm \varepsilon_V \pm \varepsilon_I)\frac{(\Delta T_{DUT} \pm 2\varepsilon_T)}{(\Delta T_{CAL} \mp 2\varepsilon_T)} \quad (4)$$

in which P_{LOSS} is the *actual* power dissipation and ε_T = 0.1 °C is the error involved in the water temperature measurements. In the first parenthesis of (4), the values of ε_I and ε_V are much smaller than unit, and thus are negligible.

Fig. 7 presents the measurement error (ε) for the proposed calorimeter for various power dissipations, when a low flow rate is applied and P_{FAN}= 0.3 W. The error band shrinks at higher P_{LOSS} values and is expanded at lower powers due to the inaccuracy of the water temperature sensors, as indicated by (4). The calorimeter is capable of tracking power losses as low as 500 mW with +50%/ -30% accuracies. The error is less

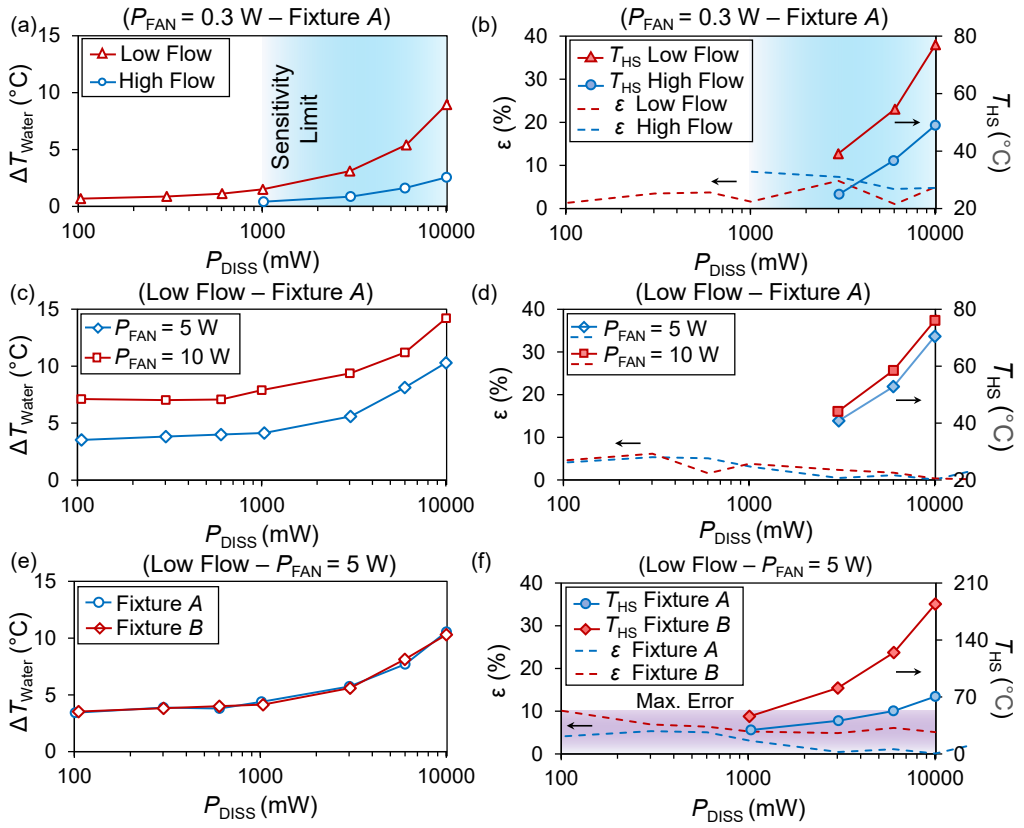

Fig. 4 Steady-state dc calibration test results for the calorimeter. (a) The effect of different water flow rates. Low flow increases the sensitivity. High flow enables better cooling of the DUT. (b) The effect of P_{FAN} at 5 W and 10 W. Increasing fan power leads to higher steady-state THS. This parameter is instrumental to converters and components that use a heatsink for cooling. (c) The effect of DUT geometry. Due to the low thermal conductivity of the fixture *B* to the cold plate, it has a much higher T_{HS}. However, ΔT_{Water} remains similar in both cases, exhibiting no dependence on DUT geometry. The mismatch errors of less than 10% for losses as low as 100 mW indicate similar designs of the two chambers and repeatability of the measurement results.

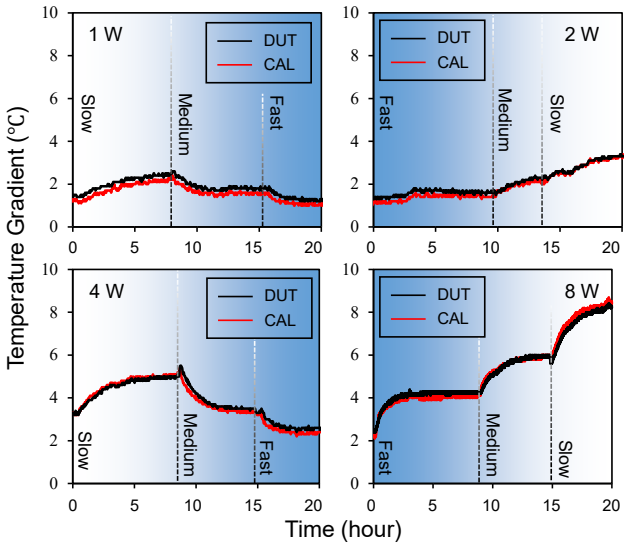

Fig. 5 DC calibration for losses from 1 W to 8 W. Temperature gradients for DUT (black) and CAL (red) are recorded. For each power level, three different flows (slow, medium and fast) are applied. The dashed lines separate between intervals of different flow rates. The inner fan power is set to 900 mW here.

than 30% for any measurements above 1 W and is significantly lower at higher power levels.

VI. System-Level Efficiency Measurement

The demonstrated calorimeter significantly improves the accuracy in system-level efficiency measurements for ultra-high-efficiency power converters in kilowatts ranges. The *actual* converter efficiency can be expressed as

$$\eta_{ACTUAL} = P_{OUT}/P_{IN} = 1 - P_{LOSS}/P_{IN} \tag{5}$$

in which P_{IN} and P_{OUT} are the *actual* average input and output powers, respectively, and P_{LOSS} is the *actual* power dissipation. For a dc-dc converter, one needs to use a high-precision digital multimeter (DMM) to measure powers P_{IN} and P_{OUT} by multiplication of currents and voltages, and then

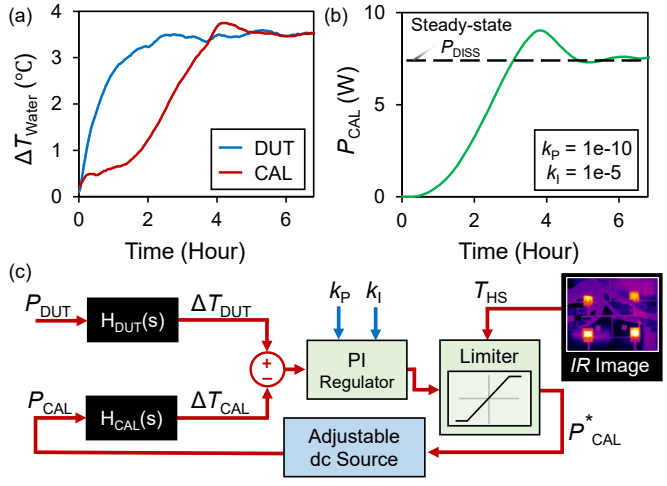

Fig. 6 System transient response and control scheme. (a) Water temperature gradients and (b) the corresponding power tracking for a 7.8-W test. (c) Controller Design. Temperature gradients are compared, and a PI regulator adjusts P^*_{CAL} to equalize the temperature gradients. An infrared (*IR*) camera provides T_{HS} to avoid device thermal runaway.

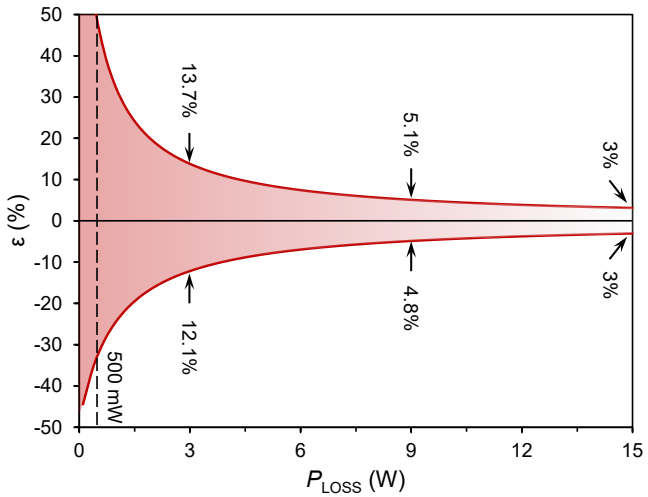

Fig. 7 Power tracking error vs. actual dissipated power when the low flow is applied. The system can measure P_{LOSS} = 500 mW (indicated by the dashed line) with an error of less than 50%. The error is significantly reduced at higher losses.

extract efficiency using (5) as

$$\eta_{DMM} = \frac{P_{OUT}(1 \mp \varepsilon_V \mp \varepsilon_I)}{P_{IN}(1 \pm \varepsilon_V \pm \varepsilon_I)} \tag{6}$$

where ε_V and ε_I represent the dc voltage and dc current measurement errors, respectively.

The main advantage of using calorimeters for efficiency measurements is that they can directly measure the P_{LOSS}, which is infeasible to do with electrical methods.

Based on (5), the calorimeter measures the efficiency of the same power converter as

$$\eta_{CAL} = 1 - \frac{P_{LOSS}(1 \mp \varepsilon)}{P_{IN}(1 \pm \varepsilon_V \pm \varepsilon_I)} \tag{7}$$

in which ε represents the calorimeter loss measurement error extracted from (4) (see Fig. 7). Fig. 8 operating at 1 kW, when using the proposed calorimeter and a high-

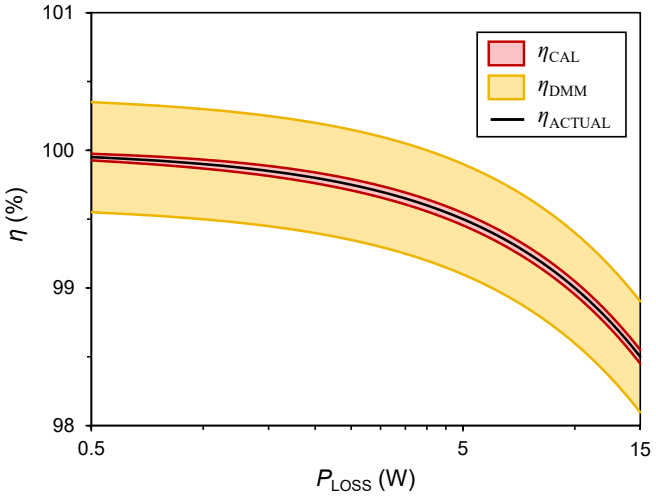

Fig. 8 Comparison of the efficiency measurements using a high-precision DMM (Fluke 87V) and the calorimeter system for a power converter operating at 1 kW. Shaded areas indicate the uncertainty ranges in each method. The calorimeter avoids spurious efficiency measurements for ultra-efficient power converters in the range of kilowatts.

Precision DMM with ε_V = 0.05% and ε_I = 0.2%. The calorimeter avoids spurious efficiency measurements for kW-range power converters with ultra-high efficiencies.

VII. Component-Level Loss Measurement

Low losses in components with high-frequency ac excitations (e.g. inductors and transformers) and fast voltage and current transitions (e.g. switches and diodes) can be very inaccurate to be measured electrically.

Power converters based on WBG technologies can expose inductors to high-frequency currents or high-dv/dt voltage excitations [7], [8], [22], [23].

A two-winding method is generally used to measure core loss, in which a transformer is made by adding a secondary sensing winding to the inductor [22]. This method is susceptible to large errors due to large phase discrepancies [24]. Although the method has been improved for phase discrepancies by introducing capacitive and inductive cancellation methods [25], still several sources of error exist, including the parasitic inductance of current measurement probe (or resistor) and interwinding and intrawinding transformer capacitances. Especially for measurement of low-permeability cores in high-quality inductors, the aforementioned errors become significant. For instance, to provide a proper coupling between the two windings of the transformer in low-permeability magnetic cores, a bifilar winding structure is necessary, which can significantly increase the interwinding capacitance.

The proposed calorimeter overcomes the aforementioned shortcomings at high frequencies (tens of MHz) and unlike most electrical methods which extract inductor losses only under sinusoidal excitations, it can measure these losses under real power circuit operation, regardless of waveforms, frequencies and transition speeds (i.e. dv/dt) applied. The only trade-off is the increased measurement times compared to electrical methods; however, the proposed calorimetric concept can save time by removing extra balance tests and compensations compared to other calorimetric methods.

In this section, we compare two toroidal inductors with similar inductance (L), for their small-signal quality factor (Q) and large-signal core and winding losses. Fig. 9a demonstrates the setup for small-signal measurements of L and Q using an E4990A Keysight impedance analyzer with 16047E 120 MHz fixture. As Figs. 9b, c present, an air-core inductor is compared with a low-permeability NiZn ferrite material (material 68). As Figs. 9d, e show, both of the inductors maintain a 6.9 µH inductance up to several MHz; however, the ferrite 68 material has a much higher Q. The small-signal Q is a measure of winding losses (especially for air-core inductors); nonetheless, a large-signal excitation is required to evaluate the overall losses, including core loss. To this end, a Gallium Nitride (GaN) inverter was used as a large-signal excitation source. Fig. 10a shows the hardware used for the experiments, including a controller board for generating PWM signals, the GaN inverter (the inset of Fig. 10a) and a resonant capacitor in series with the inductor under test.

Two sets of measurements were performed to extract the losses. In Fig. 10b configuration, the calorimeter was used to

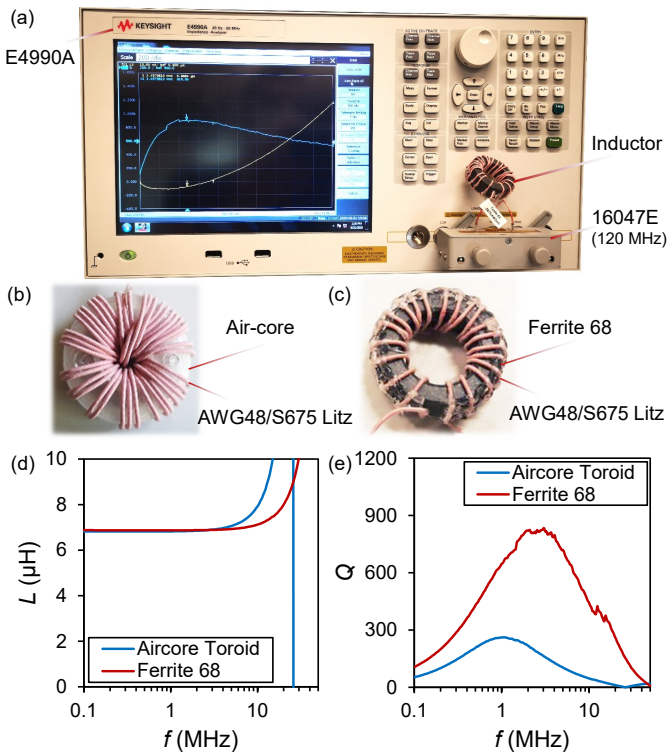

Fig. 9 (a) E4990A impedance analyzer with 16047E test fixture is used to measure the small-signal properties of two inductors with (b) an air-core and (c) a ferrite 68 core. The inductors have equal inductance several MHz. (d) shows the series inductance and (e) presents their small-signal quality factors. The amplitude of the ac signal was set to 500 mV, and the dc bias was zero.

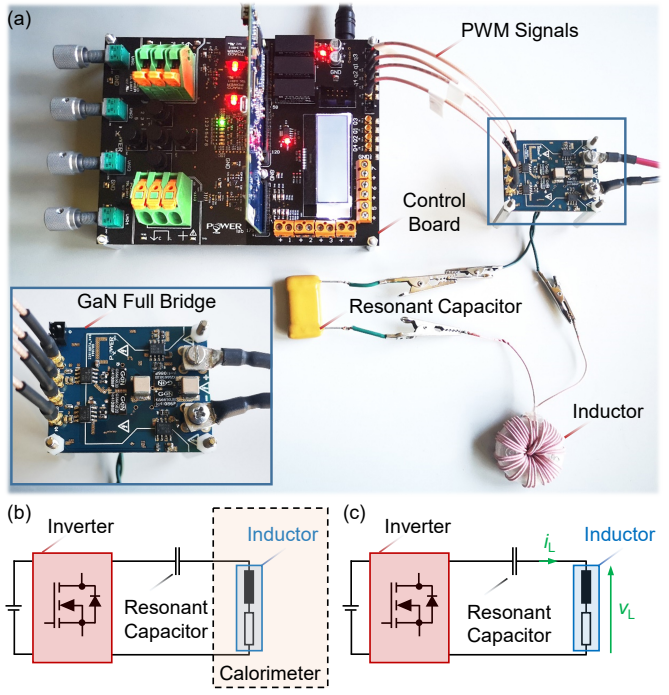

Fig. 10 Large-signal loss measurement setup. (a) a controller using TMS320F28379D DSP generates PWM signals to drive a GaN-based inverter. In order to make a resonance, the inductor was in series with a high-Q (mica) capacitor. (b) shows a setup for calorimetric measurement, and (c) shows a setup for electrical measurement using MSO64 oscilloscope with voltage (TPP1000) and current (TCPA300 Amplifier + TCP305) probes.

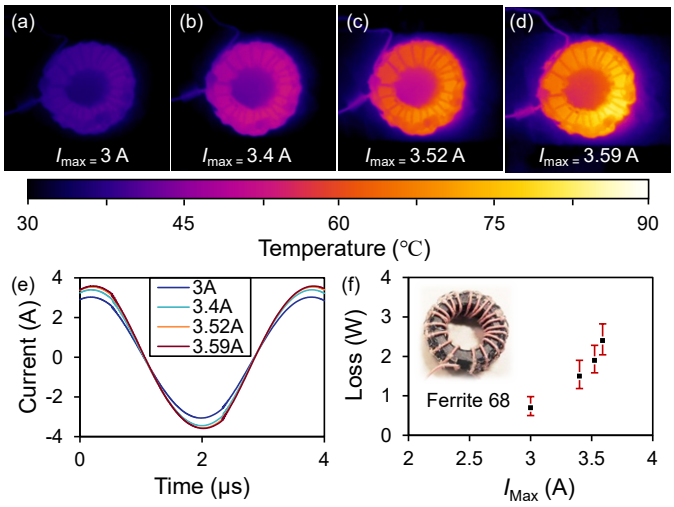

Fig. 11 Thermal measurements for the Ferrite 68 inductor. (a) to (d) present device temperatures under different peak currents ranging from 3 A to 3.59 A. (e) shows current waveforms and (f) provides the losses measured by the proposed calorimeter. The error bars are indicated for each measurement. A low water flow rate and an inner fan power of 300 mW were applied.

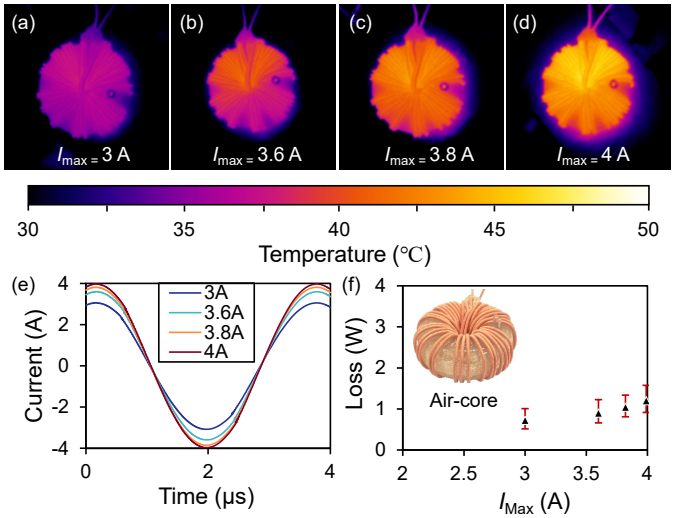

Fig. 12 Thermal measurements for the air-core inductor. (a) to (d) present device temperatures under different maximum currents ranging from 3 A to 4 A. (e) shows the current waveforms and (f) provides the losses measured by the proposed calorimeter. The error bars are indicated for each measurement. A low water flow rate and an inner fan power of 300 mW were applied.

measure inductor losses. According to the configuration in Fig. 10c, a voltage probe with 1 GHz of bandwidth (BW) and current probe with BW = 50 MHz were employed to extract the overall (core and winding) losses involved in each charging-discharging cycle of the inductors.

The calorimetric measurements are presented in Fig. 11 and Fig. 12, in which the inductors were subjected to current excitations at a fundamental frequency of 277 kHz, with different amplitudes. Figs. 11a-d present *IR* thermographs of the ferrite 68 inductor with peak currents ranging from 3 A to 3.59 A, as shown in Fig. 11e. The losses are plotted in Fig. 11d (uncertainty ranges are indicated in red). Figs. 12a-d show the *IR* thermographs of the air-core design, with peak currents ranging from 3 A to 4 A (see Fig. 12e), and losses plotted in Fig. 12d. Unlike the air-core design, ferrite 68 inductor losses increase significantly with current excitation amplitude (cf. Fig. 11f and Fig. 12f).

In parallel with each calorimetric measurement, an electrical measurement was performed to extract magnetic flux density (B) over current (see Figs. 13a-h). The B-I curves were used to calculate electrical loss as

$$P_E = f \int I dB \quad (8).$$

P_E incorporates hysteresis loss (as the major source of power dissipation in ferrite cores) and winding loss. Figs. 13i, j compare extracted losses based on calorimetric and electrical methods, and the calorimeter obtained an outstanding accuracy in loss measurements, verified by electrical measurements at a relatively low fundamental excitation frequency of 277 kHz, at which the BW of probes were sufficient. Nonetheless, for inductors operating at higher frequencies (i.e. several tens of MHz), BW limitations of probes (especially in current probing) hinder their utility. For such applications, the proposed calorimeter provides a simple, accurate and cost-effective solution to capture small losses.

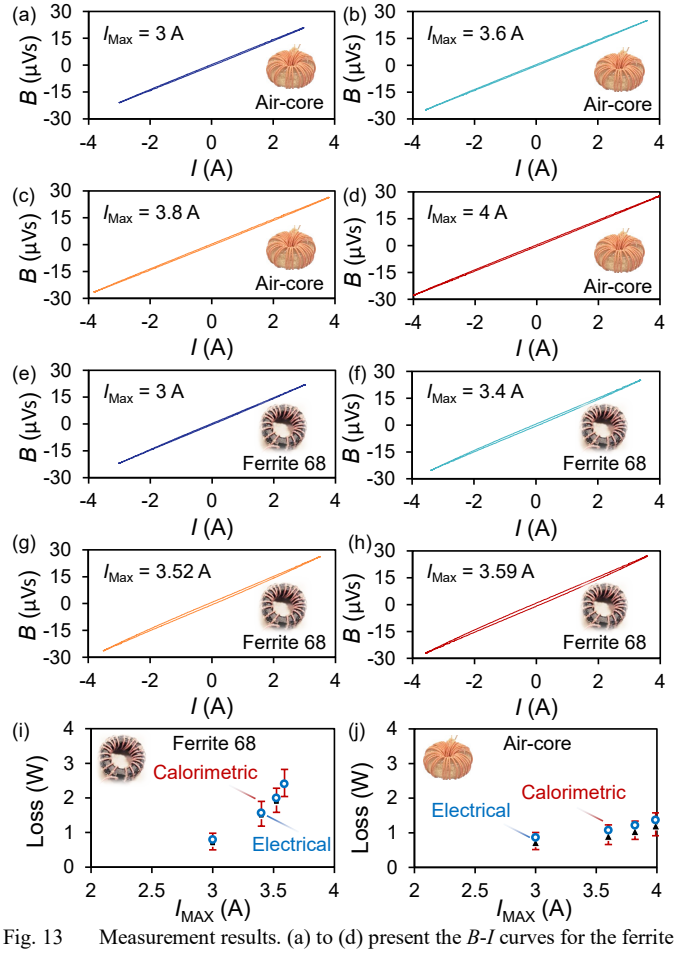

Fig. 13 Measurement results. (a) to (d) present the B-I curves for the ferrite 68 inductor with peak currents from 3 A to 3.59 A. (e) to (h) present the B-I curves for the air-core inductor with peak currents from 3 A to 4 A. (i) and (j) compare the electrical and calorimetric results. The calorimeter accuracy is verified by the electrical measurements. For inductors operating at several tens of MHz, loss measurement based on electrical methods is not feasible, due to the BW limitations of probes, especially current probes.

VIII. Conclusion

A previously-proposed closed-type dual-chamber calorimeter with an unprecedented accuracy and measurement range was analyzed in further details. The calorimeter can measure low levels of power dissipations, enabling measurement of losses down to 500 mW. The method reduces measurement time and avoids further data processing by applying a real-time calibration. The heat is transferred based on convection and conduction, enabling sensitive measurements of losses in components with various geometries and different cooling schemes. Using the same water flow in both chambers enabled very low flow rates and elimination of flowmeters, resulting in a very high accuracy and low system cost. The calorimeter offers accurate efficiency measurements for ultra-efficient converters in the range of kilowattts. It also enables precise loss measurements for power electronics components. Here, the outstanding accuracy of the calorimeter for measuring low losses in power inductors was demonstrated. Being simple, cost-effective and accurate, the proposed calorimeter concept paves the way for loss measurements in the high and very-high frequency domains, where electrical measurements are prone to inaccurate results, especially in the case of transistor switching losses and losses in magnetic components.

References

[1] A. Jafari, M. Samizadeh Nikoo, N. Perera, H. K. Yildirim, F. Karakaya, R. Soleimanzadeh and E. Matioli., "Comparison of Wide-band-gap Technologies for Soft-Switching Losses at High Frequencies," *IEEE Trans. Power Electron.*, pp. 1–1, 2020, doi: 10.1109/TPEL.2020.2990628.

[2] R. S. Yang, A. J. Hanson, B. A. Reese, C. R. Sullivan, and D. J. Perreault, "A Low-Loss Inductor Structure and Design Guidelines for High-Frequency Applications," *IEEE Trans. Power Electron.*, vol. 34, no. 10, pp. 9993–10005, Oct. 2019, doi: 10.1109/TPEL.2019.2892397.

[3] Y.- Wu, J. Gritters, L. Shen, R. P. Smith, and B. Swenson, "kV-Class GaN-on-Si HEMTs Enabling 99% Efficiency Converter at 800 V and 100 kHz," *IEEE Transactions on Power Electronics*, vol. 29, no. 6, pp. 2634–2637, Jun. 2014, doi: 10.1109/TPEL.2013.2284248.

[4] R. Ramachandran and M. Nymand, "Experimental Demonstration of a 98.8% Efficient Isolated DC–DC GaN Converter," *IEEE Trans. Ind. Electron.*, vol. 64, no. 11, pp. 9104–9113, Nov. 2017, doi: 10.1109/TIE.2016.2613930.

[5] F. Xue, R. Yu, and A. Q. Huang, "A 98.3% Efficient GaN Isolated Bidirectional DC–DC Converter for DC Microgrid Energy Storage System Applications," *IEEE Transactions on Industrial Electronics*, vol. 64, no. 11, pp. 9094–9103, Nov. 2017, doi: 10.1109/TIE.2017.2686307.

[6] A. Jafari, M. Samizadeh Nikoo, F. Karakaya, and E. Matioli, "Enhanced DAB for Efficiency Preservation Using Adjustable-Tap High-Frequency Transformer," *IEEE Trans. Power Electron.*, vol. 35, no. 7, pp. 6673–6677, Jul. 2020, doi: 10.1109/TPEL.2019.2958632.

[7] A. Jafari, M. Samizadeh Nikoo, F. Karakaya, N. Perera, and E. Matioli, "97.4%-Efficient All-GaN Dual-Active-Bridge Converter with High Step-up High-Frequency Matrix Transformer," *PCIM Europe digital days 2020, International Exhibition and Conference for Power Electronics, Intelligent Motion, Renewable Energy and Energy Management, 2020, pp. 1-8.*

[8] M. Samizadeh Nikoo, A. Jafari, N. Perera, and E. Matioli, "Efficient High Step-Up Operation in Boost Converters Based on Impulse Rectification," *IEEE Trans. Power Electron.*, vol. 35, no. 11, pp. 11287–11293, Nov. 2020, doi: 10.1109/TPEL.2020.2982931.

[9] D. Rothmund, T. Guillod, D. Bortis, and J. W. Kolar, "99.1 % Efficient 10 kV SiC-Based Medium Voltage ZVS Bidirectional Single-Phase PFC AC/DC Stage," *IEEE Journal of Emerging and Selected Topics in Power Electronics*, pp. 1–1, 2018, doi: 10.1109/JESTPE.2018.2886140.

[10] D. Christen, U. Badstuebner, J. Biela, and J. W. Kolar, "Calorimetric Power Loss Measurement for Highly Efficient Converters," in *The 2010 International Power Electronics Conference - ECCE ASIA -*, Jun. 2010, pp. 1438–1445, doi: 10.1109/IPEC.2010.5544503.

[11] K. Wang, X. Yang, H. Li, L. Wang, and P. Jain, "A High-Bandwidth Integrated Current Measurement for Detecting Switching Current of Fast GaN Devices," *IEEE Transactions on Power Electronics*, vol. 33, no. 7, pp. 6199–6210, Jul. 2018, doi: 10.1109/TPEL.2017.2749249.

[12] C. Xiao, G. Chen, and W. G. H. Odendaal, "Overview of Power Loss Measurement Techniques in Power Electronics Systems," *IEEE Trans. on Ind. Applicat.*, vol. 43, no. 3, pp. 657–664, 2007, doi: 10.1109/TIA.2007.895730.

[13] M. Sverko and S. Krishnamurthy, "Calorimetric loss measurement system for air and water cooled power converters," in *2013 15th European Conference on Power Electronics and Applications (EPE)*, Lille, France, Sep. 2013, pp. 1–10, doi: 10.1109/EPE.2013.6634469.

[14] F. Carastro, J. C. Clare, M. J. Bland, and P. W. Wheeler, "Calorimetric loss measurements and optimization of high power resonant converters for pulsed applications," p. 9.

[15] Wenping Cao, K. J. Bradley, and A. Ferrah, "Development of a High-Precision Calorimeter for Measuring Power Loss in Electrical Machines," *IEEE Trans. Instrum. Meas.*, vol. 58, no. 3, pp. 570–577, Mar. 2009, doi: 10.1109/TIM.2008.2005083.

[16] A. Kosonen, L. Aarniovuori, J. Ahola, J. Backman, J. Pyrhonen, and M. Niemela, "Loss Definition of Electric Drives by a Calorimetric System With Data Processing," *IEEE Trans. Ind. Electron.*, vol. 61, no. 8, pp. 4432–4442, Aug. 2014, doi: 10.1109/TIE.2013.2274417.

[17] T. Kleeb, B. Dombert, S. Araújo, and P. Zacharias, "Loss measurement of magnetic components under real application conditions," in *2013 15th European Conference on Power Electronics and Applications (EPE)*, Sep. 2013, pp. 1–10, doi: 10.1109/EPE.2013.6631895.

[18] P. D. Malliband, N. P. van der Duijn Schouten, and R. A. McMahon, "Precision calorimetry for the accurate measurement of inverter losses," in *The Fifth International Conference on Power Electronics and Drive Systems, 2003. PEDS 2003.*, Singapore, 2003, pp. 321–326, doi: 10.1109/PEDS.2003.1282814.

[19] A. Jalilian, V. J. Gosbell, B. S. P. Perera, and P. Cooper, "Double chamber calorimeter (DCC): a new approach to measure induction motor harmonic losses," *IEEE Trans. On energy Conversion*, vol. 14, no. 3, pp. 680–685, Sep. 1999, doi: 10.1109/60.790935.

[20] P. D. Malliband, "Design of a double-jacketed, closed type calorimeter for direct measurement of motor losses," in *Seventh International Conference on Power Electronics and Variable Speed Drives*, London, UK, 1998, vol. 1998, pp. 212–217, doi: 10.1049/cp:19980526.

[21] A. Jafari, M. Heijnemans, R. Soleimanzadeh, R. van Erp, M. Samizadeh Nikoo, E. Figini, F. Karakaya and E. Matioli, "High-Accuracy Calibration-Free Calorimeter for the Measurement of Low Power Losses," in IEEE Transactions on Power Electronics, vol. 36, no. 1, pp. 23-28, Jan. 2021, doi: 10.1109/TPEL.2020.3001001.

[22] M. Luo, "Dynamic Modeling of Magnetic Components for Circuit Simulation of Power Electronic Systems," EPF, Lausanne 2018.

[23] A. Jafari and E. Matioli "High Step-Up High-Frequency Zero-Voltage Switched GaN-Based Single-Stage Isolated DC-DC Converter for PV Integration and Future DC Grids," *PCIM Europe 2018; International Exhibition and Conference for Power Electronics, Intelligent Motion, Renewable Energy and Energy Management, Nuremberg, Germany, 2018, pp. 1-6.*

[24] M. Mu, Q. Li, D. J. Gilham, F. C. Lee, and K. D. T. Ngo, "New Core Loss Measurement Method for High-Frequency Magnetic Materials," *IEEE Trans. Power Electron.*, vol. 29, no. 8, pp. 4374–4381, Aug. 2014, doi: 10.1109/TPEL.2013.2286830.

[25] D. Hou, M. Mu, F. C. Lee, and Q. Li, "New High-Frequency Core Loss Measurement Method With Partial Cancellation Concept," *IEEE Trans. Power Electron.*, vol. 32, no. 4, pp. 2987–2994, Apr. 2017, doi: 10.1109/TPEL.2016.2573273.